Cross-talk between circRNAs and mRNAs modulates miRNA-mediated circuits and affects melanoma plasticity

Maria Rita Fumagalli[1,2,3], Maria Chiara Lionetti[2,3], Stefano Zapperi[3,4] and Caterina A.

April 12, 2019

[1]This work was supported by the AIRC grant IG 2018 ID.21558.

[21]Biophysics Institute, National Research Council - Genova, Italy.

[32]Department of Environmental Science and Policy University of Milan - Milan, Italy. Email: maria.fumagalli@unimi.it, maria.lionetti@unimi.it, caterina.laporta@unimi.it

[43]Center for Complexity and Biosystems University of Milan - Milan, Italy.

[54]Department of Physics University of Milan - Milan, Italy. E-mail: stefano.zapperi@unimi.it

Received: date / Accepted: date

Abstract

da riscrivere alla fine.... CircularRNAs (circRNAs) are non-coding RNAs which compete for microRNA (miRNA) binding, influencing the abundance and stability of other RNA species. Herein we have investigated the effect of circRNAs on mir200-ZEB1 feedback loop during phenotypic switching of human melanoma cells. We also quantified in four primary and metastatic human melanoma cells derived from the same patients the level of expression of ZEB1 circuit, We also compared the level of expression of ZEB1 in primary and metastatic samples obtained from public data depository of human melanoma and breast cancers to investigate the possible difference in ZEB1 circuit in different types of tumors. The development of in silico model allow us to recapitulate the experiments and to better understand the role of circRNAs in regulating mir200ZEB1. All together our findings show a clear strong correlation between the level of expression of ZEB1 and aggressiveness of human and breast tumors. Interestingly, analyzing human melanoma cell IgR39 during phenotypic switching we observed a dynamic expression of ZEB1 without affecting the level of circZEB1.33, which is always highly abundant. Computational model helps to understand why circZEB1.33 is constantly high during the phenotypic switch and sheds light on the molecular mechanism that tunes ZEB1-mir200 circuit.

subject classification numbers as needed.

0.1 Introduction

Cancer plasticity is an emerging properties of tumor that leads to a re-thinking of therapeutic intervention [29] [28] [26] [46] [9]. Recently, our group showed that in human melanoma the cells dynamically change their phenotype expressing dynamically epithelial to mesenchymal transition (EMT) markers through a complex network of miRNAs [44]. This allow the cells to growth or stop growing maintaining a specific proportion of EMT expressing markers in the bulk [44].

Noncoding RNAs, such as microRNAs and circular RNAs (circRNAs) are all recognized to play a key regulatory role in physiological and pathological cellular processes [22]. In this connection, circRNAs, which are single-strand endogenous noncoding RNA closed in a loop [7], are widely expressed in mammalian cells and they are differential expressed in various tissues and pathological conditions[36, 21, 16, 7**?**]. Thanks to their circular form, circRNAs are more stable than linear RNAs. Since they have been detected in exosomes and in the blood, they look like ideal biomarkers candidates [31, 37, 18, 6, 30]. In this connection, it has been recently demonstrated that there is a complex network between non coding RNAs and, in particular, circRNAs compete for micro-RNA (miRNA) binding [36, 49, 51**?** , 12]. The effect of this competition is to affect the abundance and stability of other RNAs [12]. In fact, the existence of different miRNA targets which have the same binding sites, leads to an indirect, miRNA-mediated, cross-talk between competitive endogenous RNAs (ceRNA) [42, 2, 10]. The relevance of this ceRNA circuit derives from the key role that the double-negative feedbackloop between ZEB1 and members of human mir200 family in determining EMT switching [38, 4, 48].

In the present study, we investigated the possible regulative role of circRNA in a ceRNA circuit involving epithelial to mesenchymal transition (EMT) combining experiments and computational models and data analysis. EMT represents in fact one of the key processes that the cells use to acquire a migratory phenotype in a dynamic way. The core of EMT process is the circuit that includes mRNAZEB1, miRNA200a (hsa-mir200a-3p) and SNAIL1 as external transcriptional activator [38, 4, 48]. Human gene ZEB1 can produce multiple functional RNAs including circRNAs [8, 40, 32, 13]. One of them, circ-ZEB1.33 [13] (circZEB1), comes from backsplicing of exons 2 to 4 of ZEB1 transcript variant 1 (NM_001128128)[32, 13] and contains a binding site for hsa-mir200a-3p and hsa-mir141-3p, both belonging to mir200 family [32]. The latter is a well-known post-transcriptional regulators of ZEB1 [38, 35, 20, 39, 15].

Firstly we compared the level of expression of ZEB1 circuit in human primary and metastatic melanoma cells derived from the same patient (WM115/WM266 and IgR39/IgR37 cells, primary and metastatic, respectively). Then, we checked the dynamic changes of this ZEB circuit during phenotypic switching in human melanoma IgR39 cells [44]. We also checked the level of expression of ZEB1 in samples of primary and metastatic patients stored on public depository to confirm our experimental results. Finally, to evaluate if our results were specific for melanoma only, we quantified the level of expression of ZEB1 in primary and metastatic breast cancer.

0.2 Materials and methods

0.2.1 Cell culture

IgR39 and IgR37 cells (primary and metastatic human melanoma cells, respectively) were obtained from Deutsche Sammlung von Mikroorganismen und Zellkulturen GmbH [44] and WM115 and WM266 (primary and metastatic human melanoma cells, respectively) from ATCC (codice? bisogna mettere i codici!) (mettere mia citazione due linee). All cell lines were

cultured in DMEM, 15% FBS supplemented with 1% MEM vitamin, 1% MEM aminoacid, 1% antibiotics (Penicillin/Streptomycin), 1% L-glutamine (complete medium) at 37°C in a 5% CO2 humidified environment.

0.2.2 Flow cyometry

Cells are sorted for phycoerythrin (PE) anti-human CXCR6 (Codice????, R& D System, USA). For each flow cytometry evaluation, a minimum of $4 \cdot 10^7$ cells were stained and at least $5 \cdot 10^5$ events were collected and analyzed ($4 \cdot 10^7$ cells were stained for sorting). Flow cytometry sorting and analysis was performed using a FACSAria flow cytometer (Becton, Dickinson and Company, BD, Mountain View, CA). Data were analyzed using FlowJo software (Tree Star, Inc., San Carlos, CA).

0.2.3 qRT-PCR

SNAI1, ZEB1, circZEB1 and GAPDH specific primers were designed using the primer analysis software Primer3[47] and aligned on human genomic trasnscripts using Blast [5] in order to minimize off-target effects. Divergent primers encompassing backsplicing site were designed for CircZEB1 based on fasta sequenc of hsa_circ_0004907 obtained from CircBase[13]. Primers for ZEB1 mRNA was designed on exon 7 of transcript ENST00000446923 (RefSeq NM_001128128) that is in shared by 7 of the 9 protein coding transcripts according to Ensembl database (last accessed March 2019[40]). The following primers were selected:
CircZEB1_F CCAGAAGCCAGTGGTCATGA, CircZEB1_R GTCATCCTCCCAGCAGTTCT,
ZEB1_F GAGAAGCCATATGAATGCCCA, ZEB1_R GTATCTGTGGTCGTGTGGGA,
SNAI1_F TACAGGACAAAGGCTGACAGA, SNAI1_R CGGGGCATCTCAGACTCTAG,
GAPDH_F CACATCGCTCAGACACCATG, GAPDH_R TGACGGTGCCATGGAATTTG.
Briefly, total RNA was extracted with the Guanidinium Thiocyanate-Phenol-Chloroform extraction with 1 ml of TRIzol Reagent. RNA samples were incubated for 5 minutes at room temperature. After adding 0.2 ml of chloroform in each sample, the tube was vigorously shaked and centrifuged at $12{\cdot}10^3$ x g for 15 minutes at 4°C. The aqueous phase obtained was collected and placed into a new tube and 0.5 mL of 100% isopropanol was added. After 10 minutes at room temperature samples were centrifuged at $12{\cdot}10^3$ x g for 10 minutes at 4°C. The supernatant has been removed from the tube and the pellet washed with 1 ml of 75% ethanol, vortexed briefly and again centrifuged. RNA pellet has been left air drying and resuspended in 20 μl of RNAse-free water. RNA concentration and purity was determined by using Nanodrop (Eppendorf).

Synthesis of cDNA was performed on 1 μg of total RNA reverse transcribed (RT) using Vilo IV Superscript cDNA synthesis kit (Invitrogen, CA) according to manufacturer's instructions. Real time q-RT-PCR analysis was performed using ViiI7 Real Time PCR system (Applied Biosystems). Each primer pair was tested at least in six replicates using 25ng of cDNA. The PCR-reaction included 25ng of template cDNA, 5 μM of each (forward and reverse) primers, 2 μl of RNAse-free water and 10 μl of LUNA Universal SYBR Green Mastermix (New England Biosystems), in a total volume of 20 μl. Cycling conditions were as follows: 95°C enzyme activation for 10 min, followed by 50 cycles of amplification: 15" at 95°C for denaturing, 1 min at 60°C for annealing/elongation. Quantified values were normalized against the input determined by the housekeeping human gene GAPDH. Average ΔCT was calculated for plates and averaged over replicated plates and plotted as $2^{-\Delta CT}$ using R[**?**].

0.2.4 GDC expression data

Gene expression levels in primary and metastatic tumor samples from patients were obtained from Genomic Data Commons (GDC) data portal [14] RNA-seq data. A total of 468 transcriptome profile from 465 cases classified as melanoma (primary site skin) including 103 primary tumors and 366 metastatic ones were obtained. Among these only two samples were classified as primary and metastatic tumors form the same patient (TCGA-ER-A2NF), and two samples were originated from normal solid tissue and metastatic tumor of a patient (TCGA-GN-A4U8). Regarding breast cancer, 1189 transcriptome profiles were obtained from GDC database for cases showing a primary tumor. Seven of these samples were metastatic, 111 derive from normal tissue and transcriptome of all the corresponding primary tumors were retrieved. Samples annotated by GDC as treated with neoadjuvant therapy or not meeting the study protocol were excluded. ZEB1 expression was estimated using RPKM (cosa é devi dire acronimo a cosa si riferisce) and was normalized using GAPDH as housekeeping. Note that comparing the relative expression of ZEB1 instead of absolute values allows to eliminate bias due to the normalization procedure used to obtain RPKMs values.ù Moreover, we considered as additional housekeeping ribosomal protein L19 (RPL19) and PGK2 to verify that the choice of GAPDH does not influence the obtained results (data not shown).

0.3 Results

0.3.1 Expression of ZEB1 circuit in primary and metastatic human melanoma cells

The level of expression of ZEB1, a key regulator of EMT [38, 4, 48], is modulated by the external transcription factor SNAIL1 and miRNA200 (Fig. **??**. circZEB1 is a byproduct of ZEB1 (Fig. **??**. We first checked the level of expression of mRNAs ZEB1, circZEB and SNAIL in two different cell lines obtained from two patients at two different stage of aggressiveness, primary or metastatic, by qRT-PCR (Fig. **??**). In both cell, a decreased level of expression of the circuit of SNAIL1, ZEB1 and circZEB1 occurred in metastatic cells (Fig. **??**).The grade of decrease of these factors are however dependent by the cell line, representing possibly the specific biological characteristic of each patient.

To confirm that our results were not depending by cell growing condition, we analyzed the level of expression of ZEB1 in the public depository (GDC database) for tumors classified as human melanoma (primary or metastatic) [14]. As shown in figure **??** we confirmed the decreased level of expression in metastatic samples of ZEB1. To investigate if this decrease was typical of melanoma, we analyzed the level of expression of breast cancer (primary and metastasis) in public depository (GDC database). In **??** is clearly shown that the level of expression of ZEB1 is lower in the metastatic samples with respect to the primary tumors.

0.3.2 Dynamic Expression of circZEB1 during phenotipic switching

We sorted negative IgR39 cells for CSC markers and we measured at different time (T3/T10/T20days) the level of expression of the circuit of ZEB1 by QRT-PCR . As shown in our previous paper, CSC markers can be expressed in a dynamic way with a switch of EMT genes at T3, then the growth of the cells at T10 and the off of EMT genes and the going back to the stady state at T20 sellerio2015. As shown in (Fig. **??** we observed a significant increase of mRNAs ZEB1 and SNAI1 at the overshoot (T10) and a decrease at T20 towards the steady state Fig. **??**. Regarding to circZEB1, we found high and unchanged level at the overshoot and at T20 (Fig. **??**).

0.3.3 Mathematical Model of ZEB1 circuit

To explore the ZEB circuit and the imapct of biological changes in silico...we STEFANO...soprattutto capire ruolo funzionale di cricular...

MiRNA-mediated interactions are modeled using a set of differential equation in agreement with our previous work [12], details of the model are presented in the Supplementary material. Briefly, our model comprises two kinds of post-transcriptional regulation (the binding of mRNA (T) and circRNA (C) by miRNA (μ) and circRNA creation) and two possible transcriptional regulations (promoter silencing and enhancing) (Fig.**??**a,c). In general, all these interactions but circRNA creation can involve more than two molecules with multiple binding and partial or reinforced effects (cooperativity of the binding). In accordance with biological evidences, since our aim is to reproduce ZEB1-mir200a circuit, we consider two non competing equivalent biding sites for mir200a on ZEB1 3'UTR and one on circZEB1 [3]. SNAI1 and ZEB1 repression/activation on mir200/ZEB1 promoter was modeled with using appropriate Hill functions (see. Suppl.Materials, [34, 33]). We do not model explicitly SNAI1 production/degradation considering it as a tunable external input(cfr. Fig.**??**c).

Numerical solutions of equations at steady state and Gillespie simulations were performed using Mathematica v.10 and python Stochpy library. Plot were created using Python [19] and R [**?**].

Decay rate were set according to experimental estimate as follows. MiRNA half life, experimentally estimated to range from $\approx$ 8 hours up to days, was set to $\gamma_\mu = 0.001 min^{-1}$ while mRNA half life is typically of few hours [1, 41, 50] and was set to $\gamma_T = 0.01 min^{-1}$. Since circRNA are much more stable than mRNAs, with typical half life of the order of days, closer to miRNA values [21], we set its decay rate $\gamma_C = \gamma_\mu = 0.001 min^{-1}$. Protein decay rate was set to $0.01 min^{-1}$ corresponding to estimated ZEB1 half life ($\approx 2h$ [34]). For production and interaction rates, we refer to former works and experimentally estimated rates [2**?** , 34, 12].

0.3.4 Phenomenology of the model for miRNA-mediated ceRNA circuit

We treated the contributions of the other species as a constant and implicitly including them into the decay rates.

MiRNA-mediated interactions were modeled using a set of differential equation in agreement with our previous work [12] and as described in detail in Material Methods and Supplementary materials. We consider two kind of ceRNA circuits: a more general case of one miRNA (μ) regulating two targets (mRNA, T and circRNA C) without transcription regulation layer (Fig. **??**a) and the specific case of ZEB1-mir200a network comprising transcriptional silencing of the miRNA, self-activation of the target and and external transcriptional regulator (input, (Fig. **??**c)). The introduction of self-activation and transcriptional silencing of the miRNA dramatically changes the phenomenology of the model, leading to the possibility of multistable regions (Fig. **??**b,d, see also Suppl.Material). Moreover, in our model, mRNA transcription rate can vary in a limited range of values when we consider the circuit in (Fig. **??**c), while is theoretically unlimited for circuit the more general circuit (Fig. **??**a). According to our model, at equilibrium the free mRNA (T_{eq}) and circRNA (C_{eq}) concentrations result:

$$\begin{aligned} T_{eq} &= \frac{\kappa_T}{\gamma_T(1+\mu_{eq}/\mu_T)} \\ C_{eq} &= \frac{K_C(T)}{\gamma_C(1+\mu_{eq}/\mu_C} \end{aligned} \tag{1}$$

where κ and γ are production and decay rate, μ_{eq} is the amount of free miRNA molecules while μ_T and μ_C represent the thresholds determining if C and T are highly influenced by miRNA presence (when $\mu \gg \mu_i$, bound state) or are almost free (i.e. $\mu \ll \mu_i$). These thresholds are directly proportional to the decay rate γ_i and inversely proportional to miRNA-ceRNA affinity. Thus,for a given set of parameters, species with longer half-life and higher miRNA affinity are much more influenced by miRNA, while fast-decaying or low affinity species are less sensitive to variations in miRNA concentration.

Solution reported in Eq. (1) shows that T_{eq} and C_{eq} are coupled by two factors: the presence of μ_{eq} at denominator and the circRNA production rate K_C.

Linear dependence of circRNA on mRNA concentration The simplest non-trivial case that can be considered for circRNA production rate is a direct proportionality between K_C and the mRNA (i.e. $K_C(T) = \epsilon T$). In this case it is immediate to verify that circRNA grows more than linearly with T due to miRNA coupling until miRNA contribute becomes negligible (i.e. $\mu_{eq} \text{ ¡¡ } \mu_C$).

In this scenario, we obtain that the presence of circRNA-miRNA interaction increases the amount of free mRNA, and, as a consequence, its translation for both the circuits reported in Fig. **??**. In fact, the circRNA is capable to sequestrate miRNA molecules decreasing the amount of miRNA molecules capable to bind mRNA 3'UTR. Note that in the complete circuit in Fig. **??**b, cirRNA presence increases the rage of parameters for which there exist multistability and effect of circRNA on free mRNA increases increasing mRNA expression levels thus increasing the distance between the solutions (Fig. **??**d).

Since circRNA is expected to be more stable than its linear counterpart, in our model we can consider $\mu_C > \mu_T$. Thus, for a given range of transcription rates, the mRNA can be in free state ($\mu < \mu_T$) while circRNA is bounded ($\mu > \mu_C$) and this effect is even more evident when circRNA affinity for miRNA is higher than its linear counterpart (Fig. **??**). In this case most of the cirRNA produced will be sequestrated by miRNA and will remain in bound state (Fig.**??**b), while the amount of free circRNA molecules would remain almost undetectable compared to free mRNA increase (Fig.**??**a).

Limiting reagent model A more complicated relationship between circRNA production rate and mRNA level can be obtained under the hypothesis that creation of circRNA is due to the binding of linear unspliced transcript by a given protein (Q) that favors circularization and backsplicing. If the concentration of this protein is fixed when transcription rate increases, the effective circRNA production rate could be expressed in terms of an Hill function: $Kc = \epsilon \frac{T}{T_Q + T}$, where ϵ depends on the concentration of Q and T_Q is related to T-Q binding affinity. For small transcription rates, ($T \ll T_Q$, Q abundant), the dependence of Kc on T is linear $K_C \approx \epsilon T/T_Q$, recovering the linear model presented in the previous section (Fig. **??**). However, increasing mRNA level ($T \gg T_Q$) the circRNA production rate becomes constant $K_C \approx \epsilon$. In this limit, the presence of miRNA miRNA-mediated crosstalk allows an increase of C_{eq} as a function of T_{eq} more than linear while it C_{eq} becomes constant when miRNA contribute becomes negligible (Fig. **??**).

0.4 Discussion

EMT is a complex physiological process that can help cancer progression and metastasis, involving differential expression of many genes and non coding RNAs [25, 11, 24, 29]. The feed back loop between ZEB1 and the members of mir200 family, involving transcritional and post-transcriptional regulatory is the core of EMT regulatory network [33, 38, 4, 48, 24].

EMT is a physiological process helping cancer progression and metastasis. EMT involves a complex network of genes and miRNAs [25, 11, 24]. The core of EMT is considered the ZEB1 circuit [33, 38, 4, 48, 24] and changes in its expression appears to be related to a more aggressive tumor [**?** **?** **?** **?** **?**]. A backproduct of ZEB circuit is circZEB1. In the last years, an increasing number of circRNAs are recognized to play a role in the regulation of gene expression. One of the main mechanisms of action of circRNAs is the capability to bind miRNA competing with their canonical targets [36, 49, 51, 18]. Moreover, circRNAs have been found deregulated in different tumors and their expression seems to be related to their prognosis and aggressiveness [27, 30, 45, 49, 6, 16, 43, 23].

In this context, herein, we show that the level of expression of ZEB1 in human primary melanoma with respect to metastasis either in the public depository (GDC database) and in two cell lines obtained from two distinct melanoma patients a decreased level of expression of ZEB1, SNAIL1 and circZEB1. This trend is not typical of melanoma only but hapens in breast cancer too, suggesting a general feature of metastasis. Interesting, the decrease level of expression of mesenchymal markers in samples obtained from metastasis seems to indicate that the cells switch to epithelial phenotype when they reach the metastatic site according to [**?** **?**]. Moreover, in metastatic lung it has been reported similar results [**?**].

To better investigate the switch to EMT in melanoma cells, we investigated the circuit ZEB1 during the phenotypic switching in IgR39 cells. In fact, we recently demonstrated that negative IgR39 cells for CSCs markers are able to dynamically express with an overshoot EMT markers, modulating in this way the number of CSCs in the bulk [**?**]. Accordingly, we found that the level of ZEB1 increases at the overshoot in IgR39 human melanoma cells, confirming their plastic expression of EMT markers [**?**]. However, we found a constant and high level of expression of circZEB1. To better understand the biological significance of the high level of circZEB1, we investigated with computational models two possible scenario: 1) a direct proportionality between the total transcription rate and the amount of circRNA produced (linear model); 2) the presence of a third actor that favors back-splicing (limiting reagent model). We investigated this second scenario because there are evidences of canonical spliceosome proteins playing an active role in circRNA biogenesis [**?** **?** **?**].

In the first scenario the presence of ceRNA interaction between the species would predict a linear relationship between total free mRNA amount and circRNA amount [12], even in presence of transcriptional feedback loop. In the second scenario, at low transcription rates the direct proportionality between mRNA and circRNA is preserved and this model can not be distinguished by first scenario. The fold change reduction of circZEB1 observed in metastatic cells (IgR37 and WM116) compared to the primary ones are coherent with both scenario. On the other hand, at high transcription rate, the limiting can become limiting and the two models diverge, predicting a constant level of circRNA at increasing mRNA expression. This results happens during phenotyping switching in IgR39 cells where the basal level of ZEB1is high and increased even more at the overshooting. The constant level of circZEB1 could be due thinking to the second scenario at high transcriptional rate conditions.

All together, our findings show the possible use of circZEB1 as possible biomarker of aggressiveness in melanoma.

0.5 Supplementary Information

0.5.1 Parameters selection

ZEB1 has two binding sites on mir200b-mir200a-mir429 cluster promoter, shared with ZEB2 and SNAI1[3], and has multiple E-box binding sites on its own promoter, promoting its self-activation through stabilization of SMAD complexes [17]. We model two distinct binding site of for SNAI1 and ZEB1 on both mir200 and ZEB1 and we suppose them to be independent.

0.5.2 Model description

Here we present in detail our model for ZEB1-mir200 ceRNA circuit and a more generalized framework for modeling mirRNA-mediated ceRNA circuit including multiple TFs and miRNAs binding sites.

We recall that, for sake of simplicity, we assume that the cross talk and relevant changes in species abundances is restricted to the circuit reported in Fig.1 involving a single miRNA and two RNAs targets with an external tanscriptional activator, treating the contributions of other species as a constant and implicitly including them into the decay rates.

0.5.3 TFs binding on gene promoter

In this section we will derive the occupation probability and total transcription rate for mir200 and ZEB1 promoter under the hypothesis of two non-competitive and binding sites for ZEB1 ans SNAI1 proteins.

In general, a promoter D with a single binding site can be in the free state or occupied (D^*) by its transcription factor (TF). We associate to the transcription factor A binding/unbinding rates ξ_A and δ_A.

At equilibrium, the probability that the promoter exist in free ($[D]$) or bound ($[D*]$) state are coupled by

$$[D^*] = \frac{\xi_D}{\delta_D}\,[A]^{n_A}\,[D] = \left(\frac{[A]}{[A_0]}\right)^{n_A}[D] \tag{2}$$

where n_A indicate the transcription factor cooperativity.

Imposing normalization condition $[D] + [D^*] = 1$ we obtain that $[D]$ and $[D^*]$ have the functional form of activating and inhibitory Hills functions

$$\begin{cases} [D] &= \dfrac{1}{1+([A]/[A_0])^{n_A}} = H^-(A, n_A) \\ \\ [D^*] &= \dfrac{([A]/[A_0])^{n_A}}{1+([A]/[A_0])^{n_A}} = H^+(A, n_A) \end{cases} \tag{3}$$

In our model we consider two distinct binding site for SNAI1 and ZEB1 on both mir200 and ZEB1, so that the promoter can be free, bounded by either ZEB1 or SNAI1 or in the two-TF-bounded form. Thus, states of the promoter can be expressed in terms of Hills functions for a single binding site for either ZEB1 or SNAI1 (see also [33]), and the two binding sites are coupled by normalization condition $[D] + [D^S] + [D^Z] + [D^{SZ}] = 1$.

Note that, in general, the total effective transcription rate can be calculated as $\kappa_{tot} = \sum_{i=0,n} \kappa^{i*}\binom{n}{i}[D^{i*}]$ where κ^{i*} is the transcription rate associated with state $[D^{i*}]$. Thus, it is immediate to obtain that the total transcription rate is given by

$$\begin{array}{rlll} \kappa(S,Z) = & k0 & H^-(S,n_S)H^-(Z,n_Z) & \\ & +k1_S & H^+(S,n_S)H^-(Z,n_Z) + k1_Z\, H^-(S,n_S)H^+(Z,n_Z) & \\ & +k2 & H^+(S,n_S)H^+(Z,n_Z) & \end{array} \tag{4}$$

For sake of simplicity, we consider $n_S = n_Z = 2$ for both mir200a and ZEB1. While a different choice of cooperative parameters would change the output of the model and the multistability region and the number of stable solution, it does not influence the general results obtained and the global effect of the presence of circRNA.

For mir200a the TFs act as inhibitors, and as a consequence $k0 > k1_S, k1_Z > k2$, while for ZEB1 $k0 < k1_S, k1_Z < k2$.

0.5.4 General model for ceRNA circuit

In the following we present in detail our model for miRNA mediated ceRNA circuit for a generic mRNA/circRNA couple.

MiRNA-mediated interactions are modeled using a set of differential equation in agreement with our previous work []. This model include miRNA molecules (μ), the target RNAs (T, mRNA and C, circRNA) and the corresponding miRNA-target complexes as well as an external transcription factors S and protein P produced by T.

In principle, we should define $T'_{n,\alpha}$ as the number of mRNA molecules with n miRNA bound in a specific configuration α among all the possible $\binom{M}{n}$. Thus, the total number of mRNA molecules bound by α miRNA is $T_n = \sum_n T'_{n,\alpha}$.

For each single configuration, we indicate with ξ'_{T_n} the rate of binding of a single miRNA to an mRNA molecule with $n-1$ binding sites already occupied and δ'_{T_n} is the unbinding rate of one single miRNA molecule from an mRNA with n miRNAs. These parameters can be referred to the total number of mRNA bind to n miRNA T_n using a rescaling to account for the multiplicity of the configurations. The global parameters result $\xi_{T_n} = (M-1+n)\xi'_{T_n}$ and $\delta_{T_n} = n\delta'_{T_n}$, while the decay rate is not affected by rescaling ($\gamma_n = \gamma'_n$). In the following we will consider the global parameters including the correct multiplicity and use C_1 to indicate the circRNA-miRNA complex and T_1, T_2 for mRNA with one-miRNA and two miRNA bound respectively according to ZEB1 3'UTR mir200a binding sites[3, 48]. Moreover, considering multiple miRNA binding/unbinding events occurring at the same time does not affects our reasoning, and this additional layer of complexity can be adsorbed by parameter rescaling.

The general model illustrated in Fig. 1 and Fig. 4 can be described with the following

kinetics equations

$$
\begin{aligned}
\frac{d\mu}{dt} &= \kappa_\mu - \gamma_\mu \mu - \xi_{T_1}\mu T - \xi_{C_1}\mu C + \delta_{T_1} T_1 + \gamma_{T_1}\beta_{T_1} T_1 + \delta_{T_2} T_2 + 2\gamma_{T_2}\beta_{T_2} T_2 + \delta_{C_1} C_1 + \gamma_{C_1}\beta_{Cs} C_1 \\
\frac{dT}{dt} &= \kappa_T - \gamma_T T - K_C(\epsilon, T) - \xi_{T_1} T\mu + \delta_{T_1} T_1 \\
\frac{dC}{dt} &= K_C(\epsilon, T) - \gamma_C C - \xi_{C_1} C\mu + \delta_{C_1} C_1 \\
\frac{dT_1}{dt} &= -\gamma_{T_1} T_1 + \xi_{T_1} T\mu - \delta_{T_1} T_1 - \xi_{T_2} T_2 \mu + \delta_{T_2} T_2 \\
\frac{dT_2}{dt} &= -\gamma_{T_2} T_2 + \xi_{T_2} T\mu - \delta_{T_2} T_2 \\
\frac{dC_1}{dt} &= -\gamma_{C_1} C_1 + \xi_{C_1} C\mu - \delta_{C_1} C_1 \\
\frac{dP}{dt} &= -\gamma_P P + L(\mu) T
\end{aligned}
\tag{5}
$$

where κ and γ are the synthesis and decay rates, ξ_{A_s} are the association rate between miRNA and the specie A to create the complex A_s and δ_{A_s} is the corresponding dissociation rate. The parameter β gives the probability that the miRNA molecule is recycled after the decay of the complex miRNA-target and $L(\mu)$ it the total translation rate. Note that the total translation rate $L(\mu)$ depends on the number of the miRNA that are attached to mRNA and we choose explicitly model each binding site contribution, in contrast to previous works []. A general formulation of the multiple binding sites model is reported in the subsection [].

Note that, according to previous section the synthesis rate κ_μ and κ_T can be expressed as Hills functions of TFs inshibitors/activator.

Considering the system in Eq.(5) and imposing the steady state conditions, it is straightforward to obtain implicit solutions for the free species

$$
\begin{aligned}
\mu_{eq} &= \frac{\kappa_\mu}{\gamma_\mu + G_T(\mu, M_T) T_{eq} + G_C(\mu, M_C) C_{eq})} \\
T_{eq} &= \frac{\kappa_T}{\gamma_T (1 + \mu_{eq}/\mu_T)} \\
C_{eq} &= \frac{\kappa_C}{\gamma_C (1 + \mu_{eq}/\mu_C)}
\end{aligned}
\tag{6}
$$

where we have introduced the rescaled parameters

$$
\mu_T = \gamma_T / \left(\xi_T F_T(\mu, M_T)\right) \mu_C = \gamma_C / \left(\xi_C F_C(\mu, M_C)\right) \tag{7}
$$

and $F(\mu, M)$, $G(\mu, M)$ are functions that depend on the total number of miRNA binding sites M and account for the contribution of all the bounded species. An explicit and general expression for $F(\mu, M)$ is presented in the next section.

The implicit equilibrium solution give in Eq.(6) could lead in principle to multiple positive solutions in function of the cooperativity of the Hill functions κ_μ and κ_T. When we can consider

the production rates as constant, there is only one real positive solution for the concentration of RNA species.

Note that the parameter β is essential for ceRNA crosstalk, since for $\beta = 1$ (perfectly catalytic interaction) $\widetilde{\xi_{A1_i}} = 0$ and, as a consequence, the concentration of miRNA is not influenced by its targets.

0.5.5 Multiple miRNA binding sites

In this section we will consider the general case of a mRNA having M equivalent non cooperative miRNA binding sites. Using the notation introduced in previous section, the complete system is given by

$$\begin{aligned}
\frac{d\mu}{dt} &= \kappa_\mu - \gamma_\mu \mu - \textstyle\sum_{n=1,M} \xi_n \mu T_{n-1} + \sum_{n=1,M} \delta_n T_n + \sum_{n=1,M} n\gamma_n \beta T_n \\
\frac{dT}{dt} &= \kappa_T - \gamma_T T - \xi_{T_1} T\mu + \delta_{T_1} T_1 \\
\frac{dT_1}{dt} &= -\gamma_{T_1} T_1 + \xi_{T_1} T\mu - \delta_{T_1} T_1 - \xi_{T_2} T_1 \mu + \delta_{T_2} T_2 \\
&\dots \\
\frac{dT_{M-1}}{dt} &= -\gamma_{T_{M-1}} T_{M-1} + \xi_{T_{M-1}} T_{M-2}\mu - \delta_{T_{M-1}} T_{M-1} - \xi_{T_M} T_{M-1}\mu + \delta_{T_M} T_M \\
\frac{dT_M}{dt} &= -\gamma_{T_M} T_M + \xi_{T_M} T_{M-1}\mu - \delta_{T_M} T_M
\end{aligned} \tag{8}$$

Imposing steady state condition, it is possible to solve recursively the equations

$$\begin{aligned}
T_M &= \frac{\xi_{T_M}}{\gamma_{T_M} + \delta_{T_M}} \mu T_{M-1} \\
T_{M-1} &= \frac{\xi_{T_{M-1}}}{\gamma_{T_{M-1}} + \delta_{T_{M-1}} + \xi_{T_M}\mu \left(1 - \dfrac{\delta_{T_M}}{\gamma_{T_M} + \delta_{T_M}}\right)} \mu T_{M-2} \\
&\dots
\end{aligned} \tag{9}$$

and in general

$$T_n = \frac{\xi_{T_n}}{\gamma_{T_n} + \delta_{T_n} + \xi_{T_{n+1}}\mu \left(1 - \delta_{T_{n+1}} f_M(n+1,\mu)\right)} \mu T_{n-1} \tag{10}$$

where we introduced the function

$$f_M(n,\mu) = \frac{1}{\gamma_{T_n} + \delta_{T_n} + \xi_{T_{n+1}}\mu \left(1 - \delta_{T_{n+1}} f_M(n+1,\mu)\right)} \tag{11}$$

for $n = 1, M-1$ and

$$f_M(M,\mu) = \frac{1}{\gamma_{T_M} + \delta_{T_M}} \tag{12}$$

Note that given $\delta_{T_M} f_M(M,\mu) < 1$, we obtain that $\delta_{T_n} f_M(n,\mu) < 1 \ \forall n$ and $f_M(n,\mu)$ is always positive.

In the limit of very small μ (i.e. $\mu << \mu_{T_n}$), $f_M(n,\mu) \approx 1/(\delta+\gamma)$ while for very large μ, $f_M(n,\mu) \to 0$

In conclusion, all the steady state solution for $T_M..T_1$ can be adsorbed in a factor $F(\mu, M) = (1 - \delta_{T_1} f_M(1,\mu))$, $\gamma_{T_1}/(\delta_{T_1}+\gamma_{T_1}) < F(\mu, M) < 1$.

It can be useful to derive all the species as a function of T_0

$$\begin{array}{rl} T_n & = \xi_{T_n} f_M(n,\mu)\mu\, T_{n-1} \\ & = \prod_{m=n,1} (\xi_{T_m} f_M(m,\mu)\mu)\, T \end{array} \tag{13}$$

in the limit of very small μ, only $n = 1$ gives a contribute while for very large μ all the terms give a contribute, that is $\propto 1/(1 - \delta * f)$

and the reduced system is

$$\begin{array}{rl} \frac{d\mu}{dt} & = \kappa_\mu - \gamma_\mu \mu + \sum_{n=1,M} \left((\delta_{T_n} + n\gamma_{T_n}\beta) f_M(n,\mu) - 1\right) \xi_{T_n} \mu\, T_{n-1} \\ \frac{dT}{dt} & = \kappa_T - \gamma_T T - \xi_{T_1} F(\mu, M) T \mu \end{array} \tag{14}$$

In general, when considering the production of a protein P, we have to consider the total translation rate L as the sum the of translation rates $l_{P,n}$ of T_n

$$\begin{array}{rl} \frac{dP}{dt} & = l_{P,0} T + \kappa_{P,1} T_1 + ... - \gamma_P P \\ & = \sum \kappa_{P,n} \prod_{m=n,1} (\xi_{T_m} f(m,\mu)\mu)\, T - \gamma_P P \\ & = L(\mu) T - \gamma_P P \end{array} \tag{15}$$

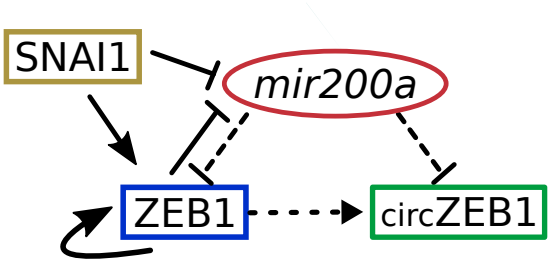

Figure 1: **ZEB1 circuit.** The circuit is composed by a miRNA–TF mutually inhibiting loop involving transcritpional (solid lines) and post-transcriptional (dashed lines) regulation. A solid arrow denotes transcriptional activation, and a solid bar denotes transcriptional inhibition. Dashed arrow connecting ZEB1 to its circRNA indicates co-generation. SNAI1 is considered as an external signal regulating ZEB1 and mir200a at transcriptional level. ZEB1 self-activation is also included.

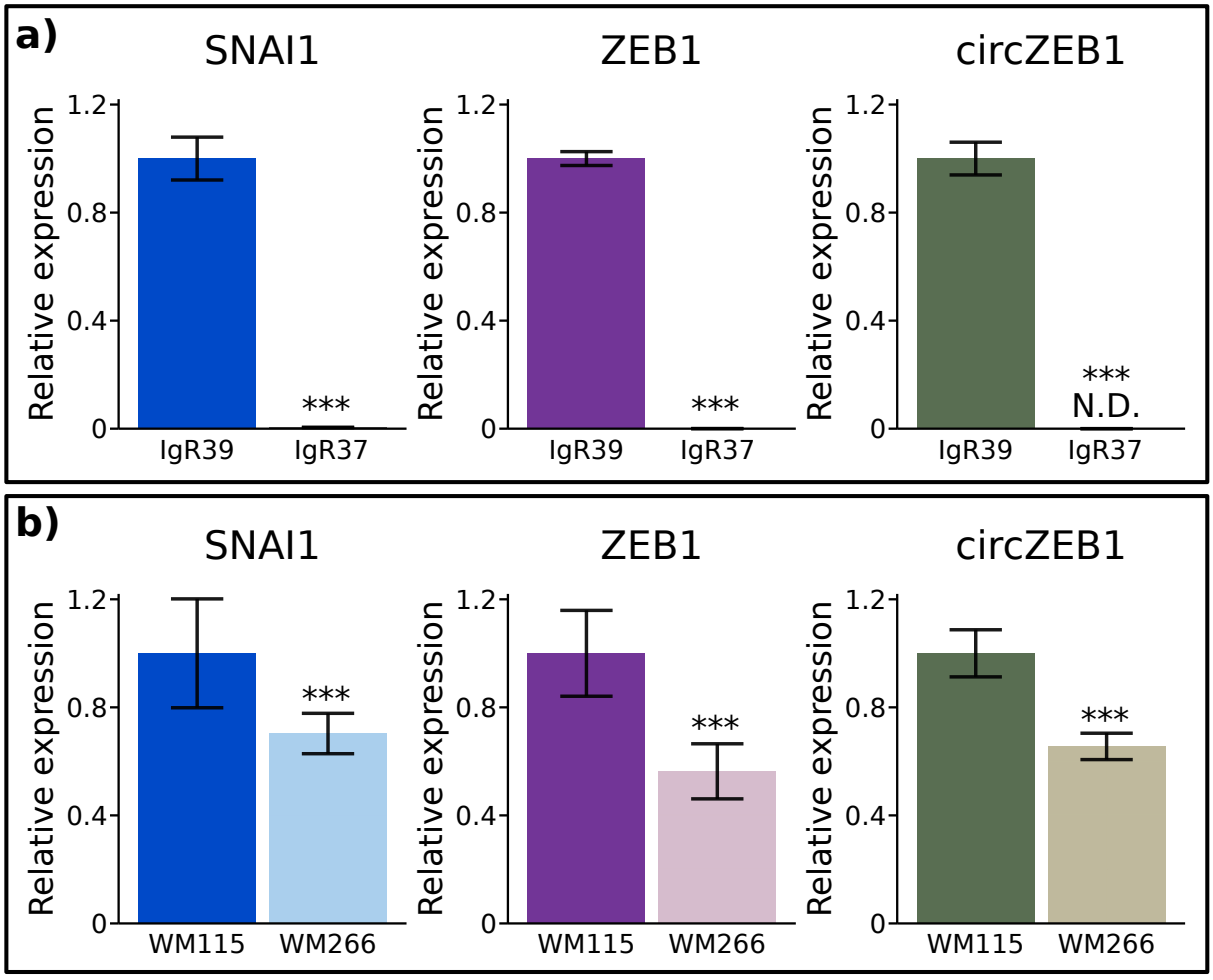

Figure 2: Expression of ZEB1, SNAIL1 and circZEB1 in primary and metastatic melanoma cell lines. qRT-PCR analysis of SNAI1 and ZEB1 and circZEB1 expression was performed in primary (IgR39 and WM115) and corresponding metastatic (WM266 and IgR37) melanoma cell lines according to Materials and Methods section. T*** $p < 0.01$ versus primary tumor IgR39 or WM115 cells. The results are expressed as $2^{\delta Ct}$ using GAPDH as housekeeping gene.

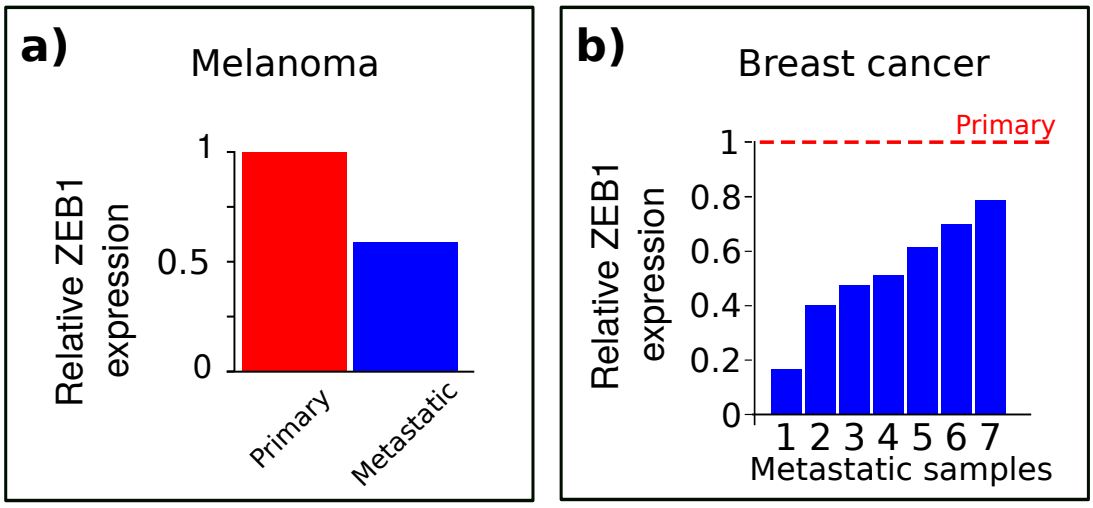

Figure 3: **ZEB1 mRNA expression in melanoma**. (a) Plot shows distribution of relative expression of ZEB1 normalized over GAPDH obtained from RNA-sequencing in 465 melanoma cases according to GDC database (see Materilas and Methods section). Data for both primary (red) and metastatic (blue) tumor samples were sorted according to increasing ZEB1 expression and x-axis was scaled in order to compare the distributions. (b) Bar plot shows the relative expression of ZEB1 in seven metastatic breast cancer samples normalized over the corresponding primary tumors from the same patients. Dashed red line indicates the normalized level of ZEB1 in primary tumor samples. Fold changes are less than one in all the samples, showing that ZEB1 expression is reduced in metastatic tumors, coherently with what observed in melanoma. Data were downloaded from GDC database as described in materials and methods section. Correspondence between x-axis label and GDC cases: 1-TCGA-BH-A1ES, 2-TCGA-AC-A6IX, 3-TCGA-BH-A1FE, 4-TCGA-E2-A15K, 5-TCGA-E2-A15A, 6-TCGA-E2-A15E, 7-TCGA-BH-A18V.

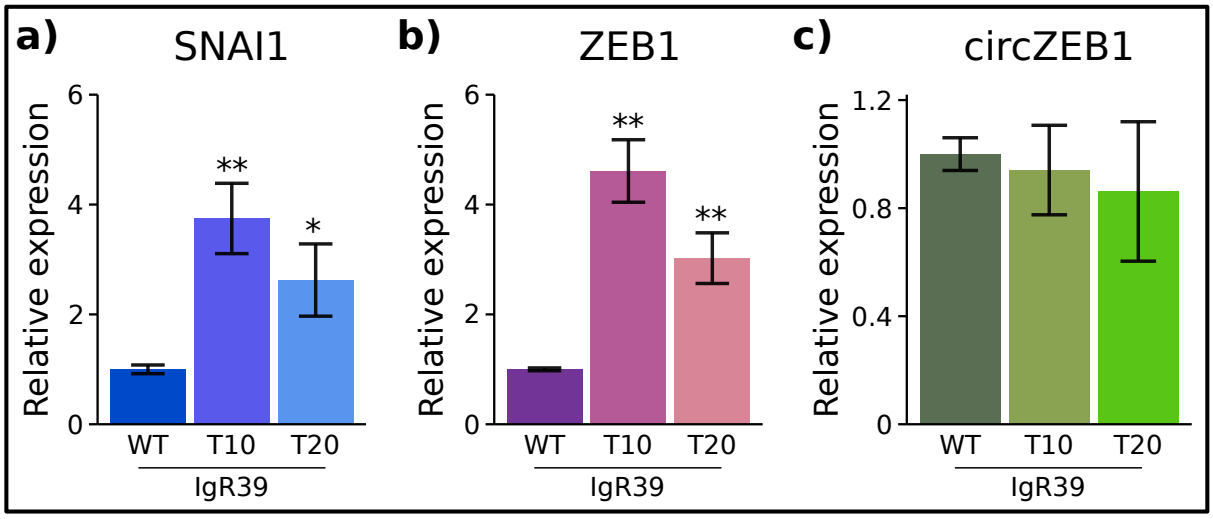

Figure 4: Level of expression of ZEB1, SNAIL1 and circZEB1 in IgR39 WT and in IgR39 CX-subpopulation 10 days and 20 days after sorting of IgR39. qRT-PCR analysis of SNAI1 (a) and ZEB1 (b) and circRNA (c) mRNa levels was carried out on sorted IgR39 negative for CSC markers as described in Materials and Methods section. * $p<0.1$, ** $p<0.05$. The results are expressed as $2^{\Delta Ct}$ vs GAPDH used as housekeeping gene.

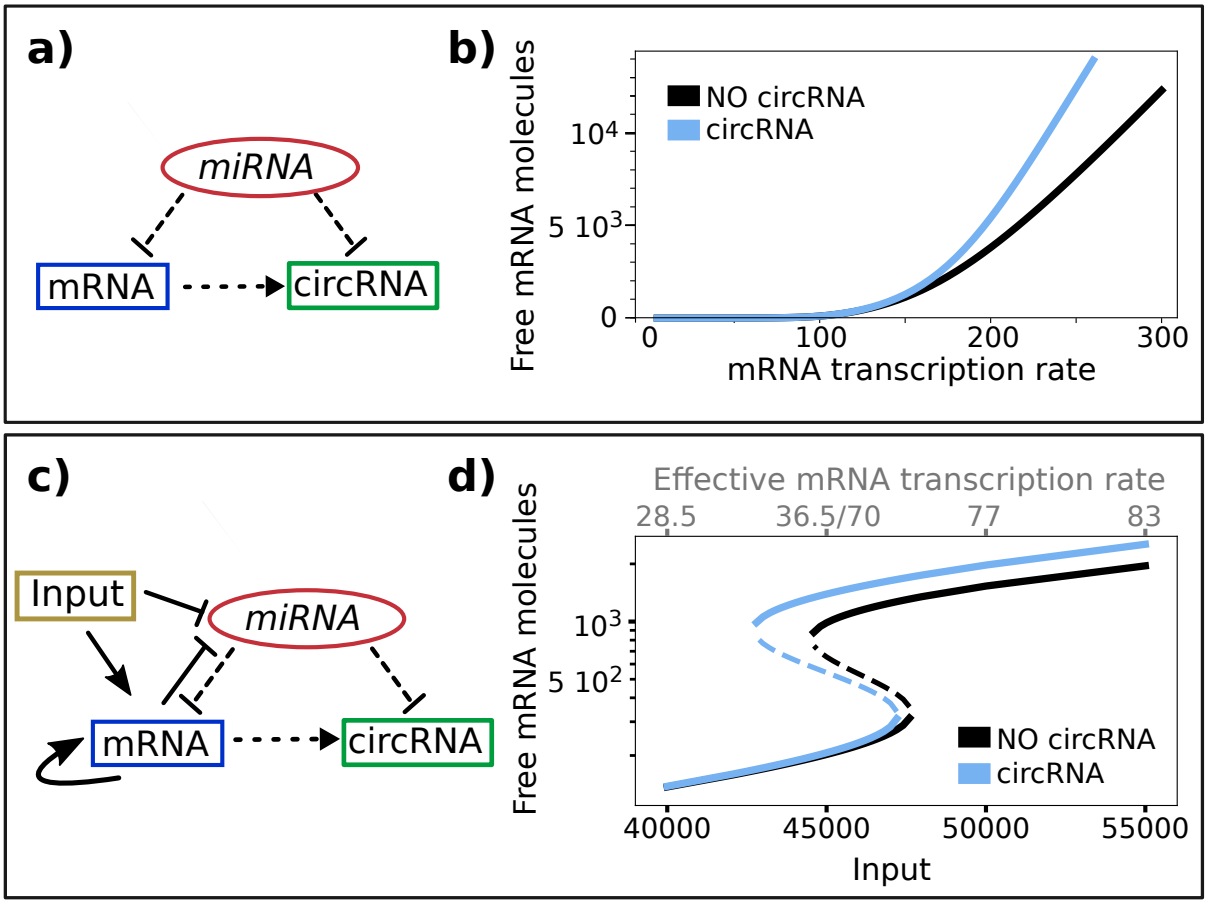

Figure 5: **Computational analysis of ZEB circuit** Figure shows two schematic representation of miRNA mediated ceRNA circuits (a,c) and numerical prediction of mRNA concentration (b,d) in presence (light blue continuous line) and absence (black line) of the circRNA. a-b) Schematic representation of the miRNA-mediated ceRNA interaction network without mRNA autoactivation and miRNA transcriptional regulation. The model predicts an increase of free mRNA molecules in presence of circRNA as a function of mRNA transcription rate (panel b). c-d) Schematic representation of the miRNA-mediated ceRNA interaction network including mRNA autoactivation and miRNA transcriptional regulation and an external regulator (c). This model resembles the ZEB1-mir200-SNAI1 circuit reported in Fig.1. This kind of circuit can present multistability, as shown in panel (d). For the choosen set of parameters, the circuit presents two stable solutions (continuous lines) and one unstable state (dashed line) at fixed input rate (lower x axis). Total effective transcription rate is reported in the upper x-axis. The level of free mRNA increases in presence of co-generate circRNA for increasing transcription rate.

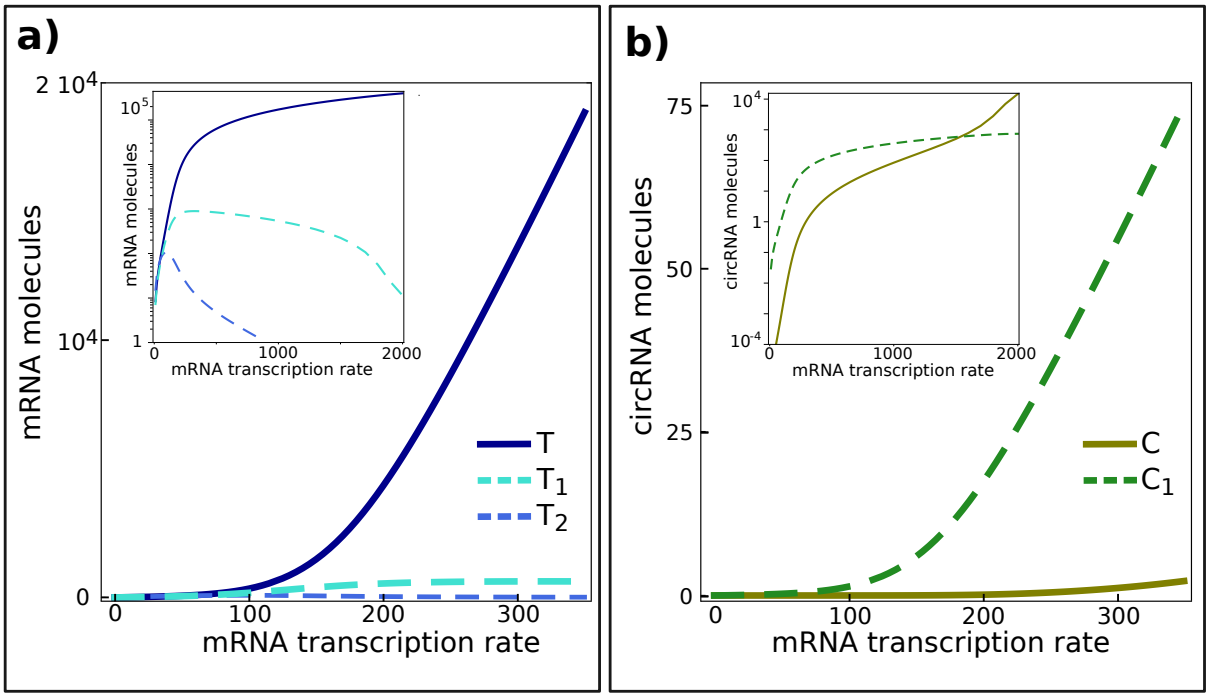

Figure 6: **CeRNAs levels as a function of mRNA production rate.** Figure shows the predicted level of free mRNA and circRNA (T and C) as well as the amount of molecules bound by one (T_1, C_1) or two (T_2) miRNA molecules according to model in Fig.1 when circRNA/miRNA affinity is larger than mRNA/miRNA affinity. For small values of mRNA transcription rate the bound forms (dashed lines) are much more abundant than free RNAs (continuous lines).Insets shows model solution at larger mRNA transcription rate. When transcription rate increases, fre mRNA becomes more abundant that bounded forms (a), while free circRNA C remains low compared to $C1$ because $\mu_C >> \mu_T$. Further increase of mRNA transcription rate leads to a decrease of miRNA molecules (not shown) and the system approach free state. The threshold transcription rate at which the cross from bounded to unbounded state is observed depends on the relative ceRNA/miRNA affinity.

Bibliography

[1] Sophie Bail, Mavis Swerdel, Hudan Liu, Xinfu Jiao, Loyal A Goff, Ronald P Hart, and Megerditch Kiledjian. Differential regulation of microrna stability. *Rna*, 16(5):1032–1039, 2010.

[2] C. Bosia, A. Pagnani, and R. Zecchina. Modelling competing endogenous RNA networks. *PLoS ONE*, 8(6):1–13, 2013.

[3] Simone Brabletz and Thomas Brabletz. The zeb/mir-200 feedback loop—a motor of cellular plasticity in development and cancer? *EMBO reports*, 11:670–7, 09 2010.

[4] U. Burk, J. Schubert, U. Wellner, O. Schmalhofer, E. Vincan, S. Spaderna, and T. Brabletz. A reciprocal repression between zeb1 and members of the mir-200 family promotes emt and invasion in cancer cells. *EMBO Reports*, 9(6):582–589, 2008.

[5] C. Camacho, G. Coulouris, V. Avagyan, N. Ma, J. Papadopoulos, K. Bealer, and T.L. Madden. Blast+: architecture and applications. *BMC Bioinformatics*, 10(421), 2009.

[6] Jie Chen, Yan Li, Qiupeng Zheng, Chunyang Bao, Jian He, Bin Chen, Dongbin Lyu, Biqiang Zheng, Yu Xu, Ziwen Long, et al. Circular rna profile identifies circpvt1 as a proliferative factor and prognostic marker in gastric cancer. *Cancer letters*, 388:208–219, 2017.

[7] L.-L. Chen. The biogenesis and emerging roles of circular rnas. *Nature Reviews Molecular Cell Biology*, 17(4):205–211, 2016. cited By 18.

[8] The UniProt Consortium. Uniprot: a hub for protein information. *Nucleic Acids Research*, 43:D204–D212, 2015.

[9] Hariharan Easwaran, Hsing-Chen Tsai, and Stephen B Baylin. Cancer epigenetics: tumor heterogeneity, plasticity of stem-like states, and drug resistance. *Mol Cell*, 54(5):716–27, Jun 2014.

[10] Matteo Figliuzzi, Enzo Marinari, and Andrea De Martino. Micrornas as a selective channel of communication between competing rnas: a steady-state theory. *Biophysical journal*, 104:1203–13, 03 2013.

[11] Francesc Font-Clos, Stefano Zapperi, and Caterina AM La Porta. Topography of epithelial–mesenchymal plasticity. *Proceedings of the National Academy of Sciences*, 115(23):5902–5907, 2018.

[12] Maria Rita Fumagalli, Stefano Zapperi, and Caterina AM La Porta. Impact of the cross-talk between circular and messenger rnas on cell regulation. *Journal of theoretical biology*, 454:386–395, 2018.

[13] Petar Glažar, Panagiotis Papavasileiou, and Nikolaus Rajewsky. Circbase: A database for circular rnas. *RNA (New York, N.Y.)*, 20, 09 2014.

[14] Robert Grossman, Allison P. Heath, Vincent Ferretti, Harold E. Varmus, Douglas R. Lowy, Warren A. Kibbe, and Louis M. Staudt. Toward a shared vision for cancer genomic data. *New England Journal of Medicine*, 375:1109–1112, 09 2016.

[15] Tianxia Guan, Claudia X. Dominguez, Robert A. Amezquita, Brian J. Laidlaw, Jijun Cheng, Jorge Henao-Mejia, Adam Williams, Richard A. Flavell, Jun Lu, and Susan M. Kaech. Zeb1, zeb2, and the mir-200 family form a counterregulatory network to regulate cd8+ t cell fates. *Journal of Experimental Medicine*, 215(4):1153–1168, 2018.

[16] Thomas B Hansen, Jørgen Kjems, and Christian K Damgaard. Circular rna and mir-7 in cancer. *Cancer research*, 73(18):5609–5612, 2013.

[17] Louise Hill, Gareth Browne, and Eugene Tulchinsky. Zeb/mir-200 feedback loop: At the crossroads of signal transduction in cancer. *International journal of cancer. Journal international du cancer*, 132, 02 2013.

[18] S Huang, B Yang, BJ Chen, N Bliim, U Ueberham, T Arendt, and M Janitz. The emerging role of circular rnas in transcriptome regulation. *Genomics*, 109(5-6):401–407, 2017.

[19] J. D. Hunter. Matplotlib: A 2d graphics environment. *Computing In Science & Engineering*, 9(3):90–95, 2007.

[20] Dimitrios Iliopoulos, Christos Polytarchou, Maria Hatziapostolou, Filippos Kottakis, Ioanna Maroulakou, Kevin Struhl, and Philip Tsichlis. Microrнas differentially regulated by akt isoforms control emt and stem cell renewal in cancer cells. *Science signaling*, 2:ra62, 10 2009.

[21] William R Jeck, Jessica A Sorrentino, Kai Wang, Michael K Slevin, Christin E Burd, Jinze Liu, William F Marzluff, and Norman E Sharpless. Circular rnas are abundant, conserved, and associated with alu repeats. *Rna*, 19(2):141–157, 2013.

[22] Jia Jia Chan and Yvonne Tay. Noncoding rna: Rna regulatory networks in cancer. *International Journal of Molecular Sciences*, 19:1310, 04 2018.

[23] Lin-hong Jiang, Da-wei Sun, Jun-chen Hou, Zhen-ling Ji, et al. Circrna: a novel type of biomarker for cancer. *Breast Cancer*, 25(1):1–7, 2018.

[24] Mohit Kumar Jolly, Marcelo Boareto, Bin Huang, Dongya Jia, Mingyang Lu, Eshel Ben-Jacob, Jose N Onuchic, and Herbert Levine. Implications of the hybrid epithelial/mesenchymal phenotype in metastasis. *Frontiers in Oncology*, 07 2015.

[25] Raghu Kalluri and Robert Weinberg. The basics of epithelial-mesenchymal transition. *The Journal of clinical investigation*, 119:1420–8, 07 2009.

[26] Antonija Kreso, Catherine A O'Brien, Peter van Galen, Olga I Gan, Faiyaz Notta, Andrew M K Brown, Karen Ng, Jing Ma, Erno Wienholds, Cyrille Dunant, Aaron Pollett, Steven Gallinger, John McPherson, Charles G Mullighan, Darryl Shibata, and John E Dick. Variable clonal repopulation dynamics influence chemotherapy response in colorectal cancer. *Science*, 339(6119):543–8, Feb 2013.

[27] LS Kristensen, TB Hansen, MT Venø, and J Kjems. Circular rnas in cancer: opportunities and challenges in the field. *Oncogene*, 37(5):555, 2018.

[28] Caterina A M La Porta and Stefano Zapperi. Complexity in cancer stem cells and tumor evolution: Toward precision medicine. *Semin Cancer Biol*, 44:3–9, 06 2017.

[29] Caterina A M La Porta and Stefano Zapperi. Explaining the dynamics of tumor aggressiveness: At the crossroads between biology, artificial intelligence and complex systems. *Semin Cancer Biol*, 53:42–47, Dec 2018.

[30] Peifei Li, Shengcan Chen, Huilin Chen, Xiaoyan Mo, Tianwen Li, Yongfu Shao, Bingxiu Xiao, and Junming Guo. Using circular rna as a novel type of biomarker in the screening of gastric cancer. *Clinica chimica acta*, 444:132–136, 2015.

[31] Yan li, Qiupeng Zheng, Chunyang Bao, Shuyi Li, Weijie Guo, Jiang Zhao, Chen Di, Jianren Gu, Xianghuo He, and Shenglin Huang. Circular rna is enriched and stable in exosomes: A promising biomarker for cancer diagnosis. *Cell research*, 25, 07 2015.

[32] Yu-Chen Liu, Jianrong Li, Chuan-Hu Sun, Erik Andrews, Rou-Fang Chao, Feng-Mao Lin, Shun-Long Weng, Sheng-Da Hsu, Chieh-Chen Huang, Chao Cheng, Chun-Chi Liu, and Hsien-Da Huang. Circnet: A database of circular rnas derived from transcriptome sequencing data. *Nucleic acids research*, 44, 10 2015.

[33] Mingyang Lu, Mohit Kumar Jolly, Ryan Gomoto, Bin Huang, Jose Nelson Onuchic, and Eshel Ben-Jacob. Tristability in cancer associated mirna-tf chimera toggle switch. *The journal of physical chemistry. B*, 117, 05 2013.

[34] Mingyang Lu, Mohit Kumar Jolly, Herbert Levine, José N Onuchic, and Eshel Ben-Jacob. Microrna-based regulation of epithelial–hybrid–mesenchymal fate determination. *Proceedings of the National Academy of Sciences*, 110(45):18144–18149, 2013.

[35] Yuhua Lu, Jingjing Lu, Xiaohong Li, Hui Zhu, Xiangjun Fan, Shajun Zhu, Yao Wang, Qingsong Guo, Lei Wang, Yan Huang, Mingyan Zhu, and Zhiwei Wang. Mir-200a inhibits epithelial-mesenchymal transition of pancreatic cancer stem cell. *BMC Cancer*, 14(1):85, Feb 2014.

[36] Sebastian Memczak, Marvin Jens, Antigoni Elefsinioti, Francesca Torti, Janna Krueger, Agnieszka Rybak, Luisa Maier, Sebastian D Mackowiak, Lea H Gregersen, Mathias Munschauer, et al. Circular rnas are a large class of animal rnas with regulatory potency. *Nature*, 495(7441):333, 2013.

[37] Sebastian Memczak, Panagiotis Papavasileiou, Oliver Peters, and Nikolaus Rajewsky. Identification and characterization of circular rnas as a new class of putative biomarkers in human blood. *PloS one*, 10(10):e0141214, 2015.

[38] Sun-Mi Park, Arti B Gaur, Ernst Lengyel, and Marcus E Peter. The mir-200 family determines the epithelial phenotype of cancer cells by targeting the e-cadherin repressors zeb1 and zeb2. *Genes & development*, 22:894–907, 05 2008.

[39] Martin Pichler, A.L. Ress, Elke Winter, V Stiegelbauer, M Karbiener, Daniela Schwarzenbacher, Marcel Scheideler, Cristina Ivan, S W Jahn, Tobias Kiesslich, Armin Gerger, Thomas Bauernhofer, George Calin, and G Hoefler. Mir-200a regulates epithelial to mesenchymal transition-related gene expression and determines prognosis in colorectal cancer patients. *British journal of cancer*, 110, 02 2014.

[40] Daniel R Zerbino, Premanand Achuthan, Wasiu Akanni, M Ridwan Amode, Daniel Barrell, Jyothish Bhai, Konstantinos Billis, Carla Cummins, Astrid Gall, Carlos García Girón, Laurent Gil, Leo Gordon, Leanne Haggerty, Erin Haskell, Thibaut Hourlier, Osagie G Izuogu, Sophie H Janacek, Thomas Juettemann, Jimmy Kiang To, and Paul Flicek. Ensembl 2018. *Nucleic acids research*, 46, 11 2017.

[41] Stefan Rüegger and Helge Großhans. Microrna turnover: when, how, and why. *Trends in biochemical sciences*, 37(10):436–446, 2012.

[42] Leonardo Salmena, Laura Poliseno, Yvonne Tay, Lev Kats, and Pier Paolo Pandolfi. A cerna hypothesis: The rosetta stone of a hidden rna language? *Cell*, 146:353–8, 08 2011.

[43] Michael Sand, Falk G Bechara, Thilo Gambichler, Daniel Sand, Michael Bromba, Stephan A Hahn, Eggert Stockfleth, and Schapoor Hessam. Circular rna expression in cutaneous squamous cell carcinoma. *Journal of dermatological science*, 83(3):210–218, 2016.

[44] Alessandro L Sellerio, Emilio Ciusani, Noa Bossel Ben-Moshe, Stefania Coco, Andrea Piccinini, Christopher R Myers, James P Sethna, Costanza Giampietro, Stefano Zapperi, and Caterina A M La Porta. Overshoot during phenotypic switching of cancer cell populations. *Sci Rep*, 5:15464, Oct 2015.

[45] Xingchen Shang, Guanzhen Li, Hui Liu, Tao Li, Juan Liu, Qi Zhao, and Chuanxi Wang. Comprehensive circular rna profiling reveals that hsa_circ_0005075, a new circular rna biomarker, is involved in hepatocellular crcinoma development. *Medicine*, 95(22), 2016.

[46] Sreenath V Sharma, Diana Y Lee, Bihua Li, Margaret P Quinlan, Fumiyuki Takahashi, Shyamala Maheswaran, Ultan McDermott, Nancy Azizian, Lee Zou, Michael A Fischbach, Kwok-Kin Wong, Kathleyn Brandstetter, Ben Wittner, Sridhar Ramaswamy, Marie Classon, and Jeff Settleman. A chromatin-mediated reversible drug-tolerant state in cancer cell subpopulations. *Cell*, 141(1):69–80, Apr 2010.

[47] Andreas Untergasser, Ioana Cutcutache, Triinu Koressaar, Jian Ye, Brant C Faircloth, Maido Remm, and Steven G Rozen. Primer3—new capabilities and interfaces. *Nucleic acids research*, 40:e115, 06 2012.

[48] G. Wang, X. Guo, W. Hong, Q. Liu, T. Wei, C. Lu, L. Gao, D. Ye, Y. Zhou, J. Chen, J. Wang, M. Wu, H. Liu, and J. Kang. Critical regulation of mir-200/zeb2 pathway in oct4/sox2-induced mesenchymal-to-epithelial transition and induced pluripotent stem cell generation. *Proceedings of the National Academy of Sciences of the United States of America*, 110(8):2858–2863, 2013.

[49] Huijun Xie, Xiaoli Ren, Sainan Xin, Xiaoliang Lan, Guifeng Lu, Yuan Lin, Shaoshan Yang, Zhicheng Zeng, Wenting Liao, Yan-Qing Ding, et al. Emerging roles of circrna_001569 targeting mir-145 in the proliferation and invasion of colorectal cancer. *Oncotarget*, 7(18):26680, 2016.

[50] Zhuo Zhang, Yong-Wen Qin, Gary Brewer, and Qing Jing. Microrna degradation and turnover: regulating the regulators. *Wiley Interdisciplinary Reviews: RNA*, 3(4):593–600, 2012.

[51] Q. Zheng, C. Bao, W. Guo, S. Li, J. Chen, B. Chen, Y. Luo, D. Lyu, Y. Li, G. Shi, L. Liang, J. Gu, X. He, and S. Huang. Circular rna profiling reveals an abundant circhipk3 that regulates cell growth by sponging multiple mirnas. *Nature Communications*, 7, 2016.